JOURNAL OF MATERIALS SCIENCE 31 (1996) 2539–2549

The relationship between the microstructure and microwave dielectric properties of zirconium titanate ceramics

F. AZOUGH, R. FREER*, C.-L. WANG, G. W. LORIMER
Materials Science Centre, University of Manchester/UMIST, Grosvenor Street, Manchester M1 7HS, UK

Zirconium titanate ($ZrTiO_4$) ceramics have been prepared by the mixed oxide route using small additions of ZnO, Y_2O_3 or CuO. Specimens were sintered mainly at 1400 °C and cooled at various rates: water-quench, air-quench, 300 °C h^{-1}, 120 °C h^{-1}, 6 °C h^{-1} and 1 °C h^{-1}. Products prepared with additives exhibited densities of at least 93% of the theoretical value. As the cooling rate after sintering was decreased, the length of the lattice parameter in the b direction was reduced and transmission electron diffraction revealed superlattice reflections associated with cation ordering. For specimens cooled at 1 °C h^{-1}, electron diffraction patterns exhibited features consistent with an incommensurate superstructure in the a direction. The dielectric Q value of rapidly cooled (air-quenched) ceramics was 2000 at 5 GHz. With an increase in the degree of cation ordering the Q value increased to a maximum of 4400 for specimens cooled at 6 °C h^{-1}. For specimens cooled at the slowest rate (1 °C h^{-1}) the Q value fell to 2000 due in part to the presence of microcracks and exsolved ZrO_2. Diffusion of trivalent impurities (yttria) into the host $ZrTiO_4$ grains also led to a lowering of the Q values.

The microwave dielectric properties of zirconium titanate ceramics are sensitive to processing conditions and mircrostructural features. The highest Q values (lowest loss) should be achieved in homogeneous specimens, free of trivalent impurities and lattice defects, in which low Q-value second phases, microcracks and pores are eliminated.

1. Introduction

During the last twenty years there has been a considerable growth in the number and types of communication systems operating in the 400 MHz–20 GHz frequency band [1]. Many circuits operating at microwave frequencies include a filter, in the form of a resonant cavity. Traditionally, air-filled cavities have been employed for such applications but Richtmyer [2] showed that unmetallized dielectrics can function successfully as resonators. There are, in fact, considerable benefits in using solid dielectrics of relative permittivity ε_r since the size of the resonator can be reduced to $1/(\varepsilon_r)^{1/2}$ of that of an air-filled cavity. The primary requirements of any resonator material are low dielectric loss, tan δ (more conveniently described in terms of high Q, where $Q = 1/\tan\delta$), high relative permittivity (to minimize component size) and a very low temperature coefficient of resonant frequency τ_f (to ensure temperature stability of operation). Rutile (TiO_2, which has a relative permittivity of ~ 100) was one of the earliest candidate dielectric ceramics for microwave applications [3], but was rejected because of its high τ_f value of 400 ppm/°C. Within the last decade, five major families of microwave dielectric ceramics have emerged, many of them including TiO_2 as a major component [4].

Zirconium titanate (ZT)-based ceramics are currently amongst the most widely used microwave dielectrics because they offer good dielectric properties and can be processed comparatively easily [5–8]. Significant additions of SnO_2 are required to provide materials with the highest temperature stability [5]. The "pure" end-member $ZrTiO_4$ has been known for over 50 years [9]. Newnham [10] showed that the crystal structure was that of α-PbO_2, with orthorhombic symmetry and the space group Pbcn. It was generally believed that the cations Zr^{4+} and Ti^{4+} were randomly distributed within the lattice. McHale and Roth [11] subsequently demonstrated that the length of the b axis was sensitive to sintering conditions. For samples sintered at ~ 1500 °C and annealed at lower temperatures there was a significant change in the cell parameters at 1125 ± 10 °C. This was described as a "structural phase transition temperature". Specimens heat-treated above this temperature had a "long" unit cell parameter in the b direction of

* Author to whom correspondence should be addressed.

0022–2461

~ 0.550 nm whilst those annealed below this temperature has "short" unit cell parameter of ~ 0.535 nm. The transition between the "high temperature" and "low temperature" forms of $ZrTiO_4$ is now believed to reflect a transition from a structure in which the cations are disordered to one in which there is some degree of cation ordering [12–18].

There is now a growing body of data which suggests that the dielectric properties of ZT-based ceramics are sensitive to the processing conditions, impurities, sintering aids and additives [6–8]. The present study was undertaken to investigate the effects of selected additives (ZnO, Y_2O_3 and CuO) and heat treatment conditions on the microstructure and microwave dielectric properties of zirconium titanate ceramics. Zinc oxide is a common additive for titanium-based electronic ceramics because of its ability to promote liquid phase sintering. The combination of ZnO and CuO has also been recommended as a sintering aid for dielectric ceramics [19]. Yttrium oxide was employed to test the proposal of McHale and Roth [12] that Y_2O_3 increases the ordering rate of ZT ceramics. A primary objective was to understand the factors which control the dielectric Q value of zirconium titanate ceramics.

2. Experimental procedure

Ceramics specimens were prepared by the classical mixed oxide route.

2.1. Materials and preparation

The starting materials were ZrO_2 (E20 grade), TiO_2 (A-HR), ZnO (analar grade), CuO (technical grade) and Y_2O_3 (analar grade). The following compositions were chosen for investigation:

(A) $ZrTiO_4$ (undoped, without additives),
(B) $ZrTiO_4$ + 1.5 wt % ZnO,
(C) $ZrTiO_4$ + 1.5 wt % ZnO + 1.0 wt % Y_2O_3,
(D) $ZrTiO_4$ + 1.0 wt % ZnO + 1.0 wt % Y_2O_3 + 0.5 % CuO.

The oxides for the desired compositions were mixed wet for 8 h, calcined at 1100 °C for 4 h and milled again for 12 h. Pellets were pressed at 120 MPa in the shape of discs of 16 mm diameter and 9 mm thick. The pellets were sintered at 1400 °C for 4 h in air and cooled at various rates: water-quenched, air-cooled, 300, 120, 6 and 1 °C h^{-1}. Selected samples of composition D were sintered at 1450 °C.

2.2. Characterization of powders and products

The density of each specimen was determined after sintering.

X-ray diffraction analysis, employing CuK_α radiation and a Philips diffractometer with a horizontal goniometer, was used to examine calcined powders and sintered specimens. The samples were scanned at 0.05° intervals of 2θ in the range 10–120°. Lattice parameters were determined from d-spacings of (0 0 2), (0 2 0), (2 0 0), (0 2 2), (2 0 2) and (2 2 0) reflections.

Prior to microscopic examination, the ceramics were ground (to 1200 grade SiC) and polished (to 1 μm diamond paste, and with Struers OPS solution). Selected specimens were chemically etched using sulfuric acid (30 s for partial etch; 10 min for full etch). Product morphologies and microstructures were examined by optical microscopy and scanning electron microscopy (SEM). Average grain sizes were determined using the linear intercept method [20].

Chemical analyses of individual grains were determined using the energy dispersive (EDS) X-ray analysis facility on the SEM (Philips 505).

Samples for transmission electron microscopy (TEM) were prepared from 3 mm diameter discs which were ground to 200 μm thickness. The centres were reduced to 30 μm thickness by a mechanical dimpling method. Final thinning for TEM was carried out on an Edward IBMA or Ion Tech ion beam thinner with Ar ions at 4–6 kV. A Philips EM430 transmission electron microscope was used for microstructure and electron diffraction studies.

High frequency dielectric measurements were performed at 5 GHz (25 °C) on polished discs (13 mm in diameter, 7 mm thick), with a network analyser and sweep oscillator (Hakki and Coleman [21] method). The resonant cavity comprised two 100 mm diameter polished copper plates with the specimen located centrally between them. Measurements were made in the transmission mode. The system was calibrated using a set of standard specimens prior to analysis of the ZT ceramics. The relative permittivity and dielectric loss were obtained from the resonant frequency and the width of peak of the TE_{011} resonant mode, using the methods of Hennings and Schnabel [22].

3. Results

Calcined powders of ZT ceramics of all four compositions were white in colour. XRD spectra for all the calcined powders showed that although the $ZrTiO_4$ phase had started to form, ZrO_2 and TiO_2 were still present. (1 1 0) and (1 1 1) zirconium titanate peaks were identified in spectra for all calcined specimens.

Sintered products of all compositions, when cooled quickly (water quenched and air quenched), were light brown in colour. With slower cooling the colour became lighter and tended to a yellow–cream.

All the ZT ceramics showed a weight loss of sintering. At cooling rates of $\geqslant 120$ °C h^{-1}, the weight loss of specimens was typically 0.5 wt %. At slower cooling rates (6 and 1 °C h^{-1}), the weight loss of specimens prepared with ZnO additions increased to a maximum value of 1.9 wt % (in compositions B and C). ZT ceramics prepared without additives were of low density typically 60–63% of the theoretical density. Sintered specimens of composition B, C and D showed densities generally greater than 93% of the theoretical value for all cooling rates. The final densities of compositions B and C were identical at a given cooling rate, but ceramics of composition D exhibit marginally higher densities up to 96% theoretical (Fig. 1).

The X-ray diffraction (XRD) spectra for fired specimens of all compositions were similar but exhibited

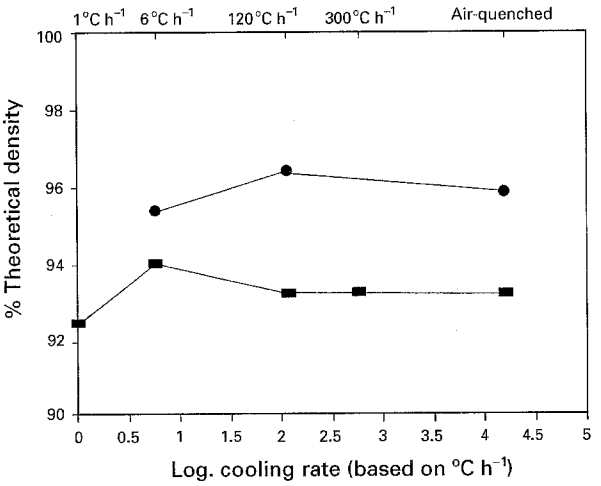

Figure 1 Fired densities of ceramics of composition B (■) and composition D (●) as a function of cooling rate after sintering. For each datum point, the typical uncertainty (one standard deviation) is ± 0.1 wt %.

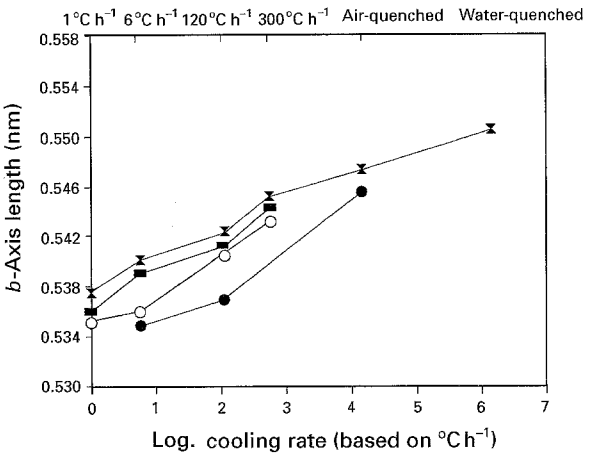

Figure 3 Length of the *b*-axis of the unit cell for zirconium titanate-based ceramics as a function of cooling rate after sintering (▼ composition A; ■ composition B; ○ composition C; ● composition D).

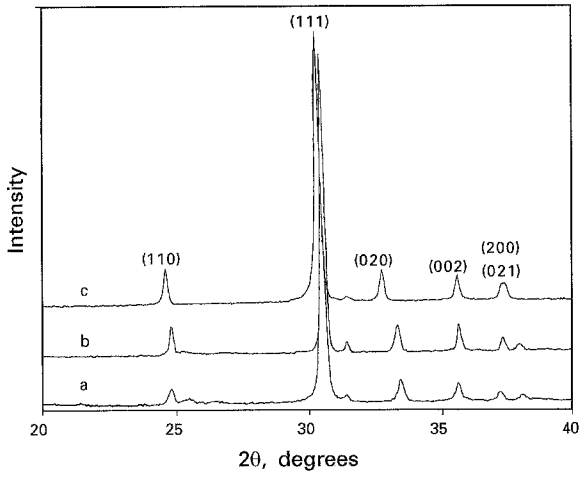

Figure 2 X-ray diffraction spectra for ceramics of composition D subjected to different cooling rates after sintering: (a) air-quenched; (b) cooled at 120 °C h^{-1}; (c) cooled at 6 °C h^{-1}.

important minor variations as a function of cooling rate. Additional peaks were observed in the spectra of samples cooled at 1 °C h^{-1}. The XRD spectra of composition D specimens cooled at different rates after sintering are shown in Fig. 2.

Structural changes accompanied the changes in the cooling rate. The length of the longest unit-cell dimension (b-axis) decreased with the decrease in cooling rate (Fig. 3), whilst the length of cell edges in the *a* and *c* directions were essentially independent of processing conditions (0.482 nm for *a* and 0.5035 nm for *c*).

The microstructures of all the ZT samples were found to be sensitive to heat treatment. Fig. 4 shows optical micrographs of ZT ceramics of composition B cooled at various rates after sintering. In the air-quenched samples, grains were rounded and uniform in shape, and the pores were uniformly distributed (Fig. 4(a)). For samples cooled at 120 °C h^{-1}, (the conventional rate) a uniform distribution of pores is also seen (Fig. 4(b)), but the grains are slightly distorted and there was evidence of transgranular cracking. As the cooling rate was further decreased, there was no significant change in the pore distribution but the distortion of the grains and the amount of internal cracks increased markedly (Fig. 4(c)).

Optical micrographs of ceramics of composition C fired at the same rates as those for specimens of composition B were similar to those shown in Fig. 4. Microstructures of ceramics of composition D were also similar but the grain size was smaller than those for other compositions prepared under identical conditions. The average grain sizes for specimens of composition B and D are given in Table I.

In the ZT specimens prepared with ZnO additions (composition B) a second phase was observed at the grain boundaries. In the air-quenched samples the second phase formed a continuous layer at the grain boundaries. As the cooling rate after sintering was decreased, the second phase formed individual grains (similar to that shown in Fig. 5), and the volume fraction of second phase decreased. When the cooling rate was 1 °C h^{-1}, the amount of Zn-bearing second phase decreased remarkably and only isolated large grains were observed (e.g. Fig. 6(a)). EDS analysis indicated the second phase was rich in Zn and Ti, with $ZnO:TiO_2$ ratio approximately 1:1 (Fig. 6(b)). Throughout the two series of specimens prepared with ZnO additions (B and C), the composition of the second phase was independent of cooling rate.

In ceramics of composition D, the second phase was rich in Zn, Ti and Cu with a small amount of Zr, i.e. 43.2 mole % ZnO, 40.4 mole % TiO_2, 13.0 mole % CuO and 3.5 mole % ZrO_2. Again the composition was independent of sample processing conditions.

The optical micrographs revealed evidence of microcracks and associated nodular particles in ceramics of composition B cooled at 120 °C h^{-1} or less and ceramics of composition B and D cooled at 1 °C h^{-1}. The form and size of these microcracks can be seen clearly in SEM micrographs of samples of composition B cooled at 120 °C h^{-1} and 1 °C h^{-1}, Fig. 7(a) and (b) respectively. The longer cracks were observed in the specimens cooled at the slower rate.

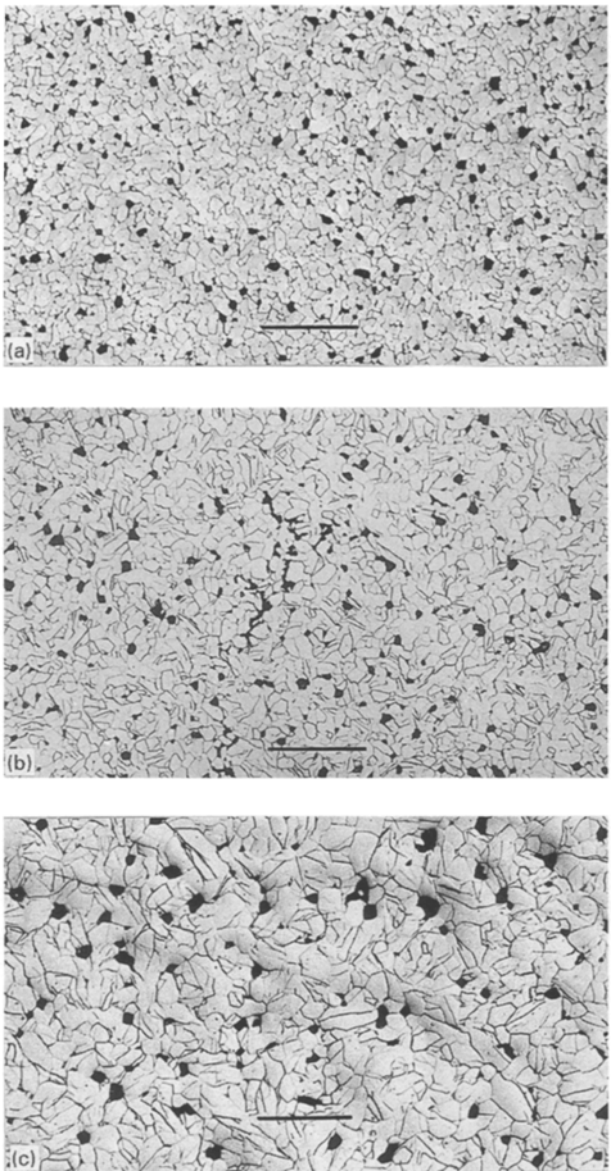

Figure 4 Optical micrographs of ceramics of composition B, cooled at different rates after sintering: (a) air-quenched; (b) cooled at 120 °C h^{-1}; (c) cooled at 1 °C h^{-1}. The rounded dark regions are porosity. Scale bars = 100 μm.

TABLE I The average grain size of ceramics compositions B and D prepared with various cooling rates after sintering at 1400 °C

Cooling rate (°C h^{-1})	Average grain size (μm) (composition B)	Average grain size (μm) composition D
Air-quenched	7 ± 2	4.7 ± 0.5
120	7 ± 2	5.3 ± 0.7
6	9 ± 3	7.2 ± 0.7
1	20 ± 5	10.2 ± 0.6

The nodular particles which can be seen in Fig. 7(b) are Zr-rich (Table II) and have a complicated internal structure when examined by TEM (Fig. 8). The primary features are a matrix which is predominantly tetragonal zirconia, and contains twinned laths of monoclinic zirconia. TEM observations of slowly cooled samples showed the presence of voids at the grain boundaries (Fig. 9).

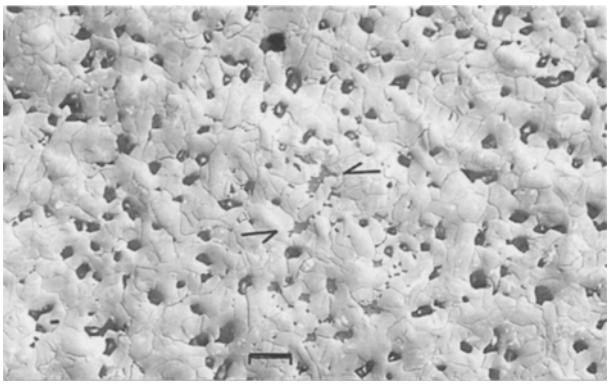

Figure 5 Optical micrograph for ceramic of composition B (cooled at 6 °C h^{-1} after sintering) showing the matrix and second phase (arrowed). Note the presence of excessive amounts of microcracks in the matrix. Scale bar = 50 μm.

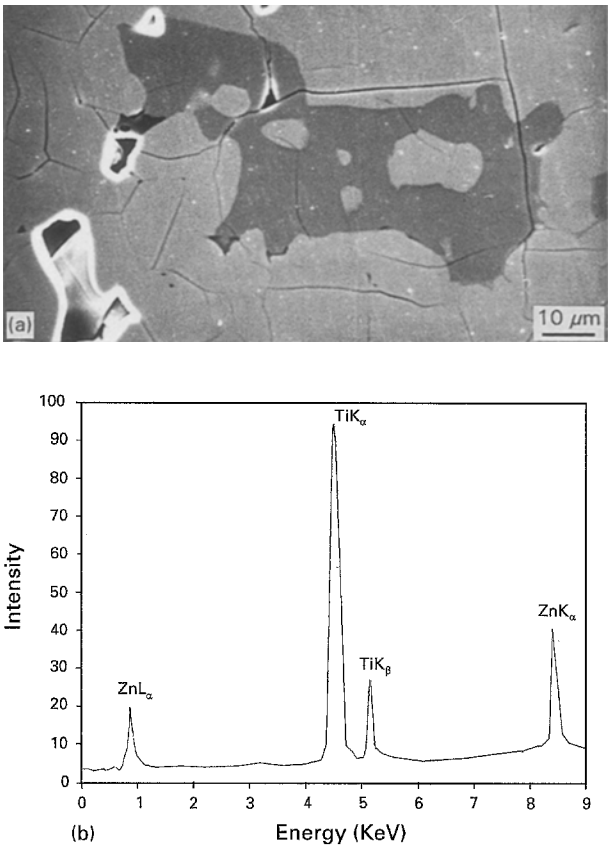

Figure 6 (a) SEM micrograph of ceramic of composition B (cooled at 1 °C h^{-1} after sintering) showing the matrix and second phase (dark region). Microcracks pass through the matrix and second phase. (b) EDS spectrum and chemical analysis of the second phase shown in (a). ZnO 53 wt %; TiO_2 47 wt %.

TEM studies confirmed that there were major differences between the rapidly and slowly cooled samples. Electron diffraction patterns of the slowly cooled ceramic revealed the presence of a superstructure in the *a*-direction. Fig. 10 shows [0 1 1] electron diffraction patterns of sample B, the zirconium titanate ceramic prepared with ZnO additions. Fig. 10(a) of an air-quenched sample shows a [0 1 1] matrix pattern which exhibits discontinuous, low intensity streaks in the *a*-direction. Fig. 10(b) shows the diffraction pattern of a sample cooled at 1 °C h^{-1}; as well as the

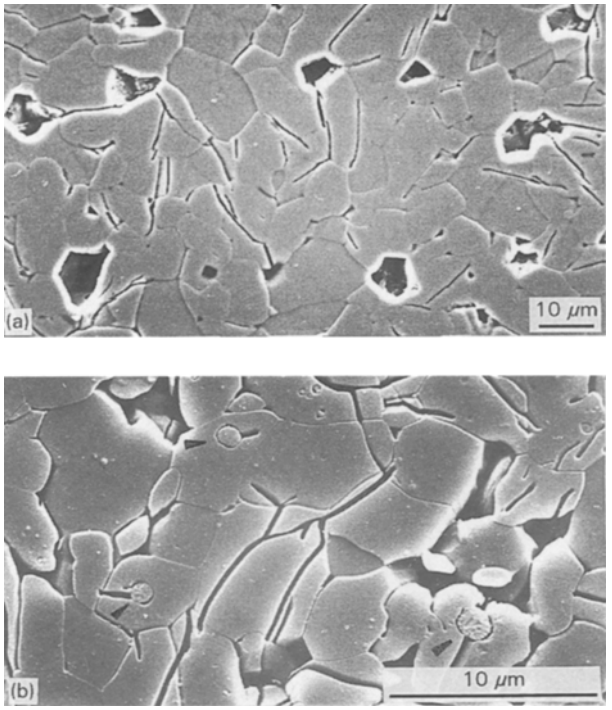

Figure 7 (a) SEM micrograph of ceramic of composition B (cooled at 120 °C h^{-1} after sintering) showing the presence of microcracks. (b) SEM micrograph of ceramic of composition B (cooled at 1 °C h^{-1}) showing microcracks and nodular particles within the grains.

TABLE II Chemical analysis of the exsolved nodular particles in zirconium titanate ceramics cooled at 1 °C h^{-1}

Oxide mol %	Composition B	Composition C	Composition D
ZrO_2	86.6	78.2	74.9
TiO_2	13.4	19.4	25.1
Y_2O_3	–	2.4	–

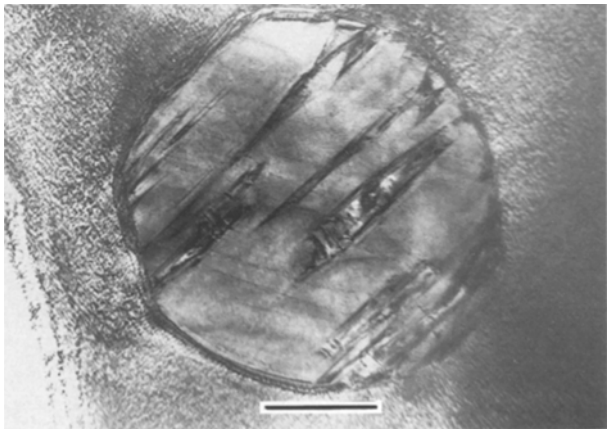

Figure 8 TEM micrograph of ceramic of composition C (cooled at 1 °C h^{-1} after sintering) showing a Zr-rich nodular particle. The particle is twinned. Scale bar = 0.5 μm.

matrix spots shown in Fig. 10(a), two types of extra reflections can be seen and there is continuous streaking in the *a*-direction (a schematic representation of the electron diffraction pattern shown in Fig. 10(b) is given in Fig. 10(c)). This type of electron diffraction

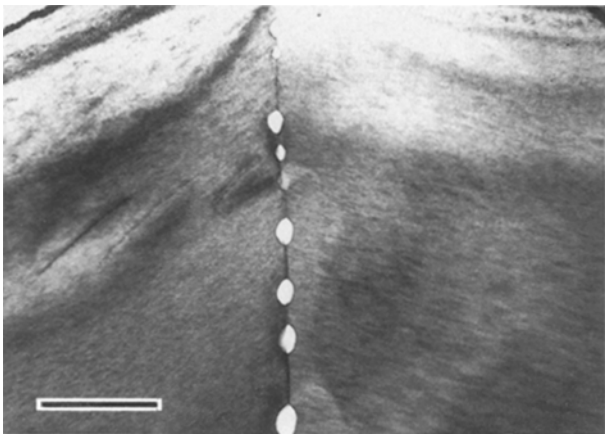

Figure 9 TEM micrograph of ceramic of composition B (cooled at 6 °C h^{-1} after sintering) showing voids at the grain boundary. Scale bar = 0.5 μm.

pattern was observed in ceramics of all compositions cooled at 1 °C h^{-1}. TEM electron diffraction patterns of samples cooled at 120 and 6 °C h^{-1} showed less intense superlattice spots and more extensive streaking than samples cooled at 1 °C h^{-1} (Fig. 11).

A sample of composition B was annealed at 1000 °C for 1000 h. The [0 1 2] electron diffraction pattern of this sample is shown in Fig. 12. Only one type of extra reflection was observed which was associated with a superstructure having a doubled *a*-axis. Continuous streaking in the *a*-direction can also be seen in the diffraction pattern. A typical high resolution TEM micrograph of sample D (cooled at 6 °C h^{-1}) is shown in Fig. 13.

Undoped zirconium titanate ceramics (composition A) exhibited low relative permittivities in the range 27.4–29.2, with a maximum for the air-quenched specimens. The *Q*-values of ceramics of this composition were also poor, between 500 and 700 for all cooling rates. The relative permittivities of materials of composition B (prepared with ZnO additions) are shown in Fig. 14. The relative permittivities of ceramics of compositions C and D are similar to those for specimens of composition B and exhibits similar trends as a function of cooling rate. The *Q* values of ceramics of composition B ($ZrTiO_4$ + 1.5 wt % ZnO) are shown in Fig. 15. For comparison purposes, data for $(Zr_{0.8}Sn_{0.2})TiO_4$ prepared with addition of 1.5 wt % ZnO are also included. For ZT, the highest *Q*-value of 4500 (at 5 GHz) was obtained with samples cooled at a rate of 120 °C h^{-1}. Rapidly cooled and more slowly cooled samples had lower *Q* values of 2000 and 2200 respectively. In contrast, the *Q* value of the ZTS samples increased as specimen cooling rate decreased. The ε_r and *Q* value (at 5 GHz) of the ZT sample annealed for 1000 h at 1000 °C were 34.5 and 2000, respectively. For ceramics of compositions C and D, the *Q* values were low, typically 500–800 for all the samples prepared at different cooling rates.

4. Discussion

4.1. The fired densities of ZT ceramics

The undoped ZT ceramics sintered at 1400 °C had a density of 63% of the theoretical value. This

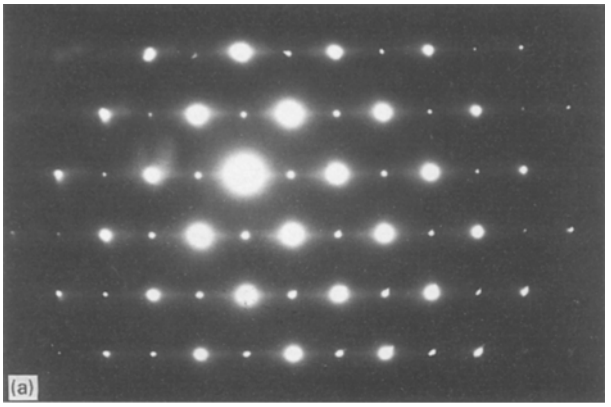

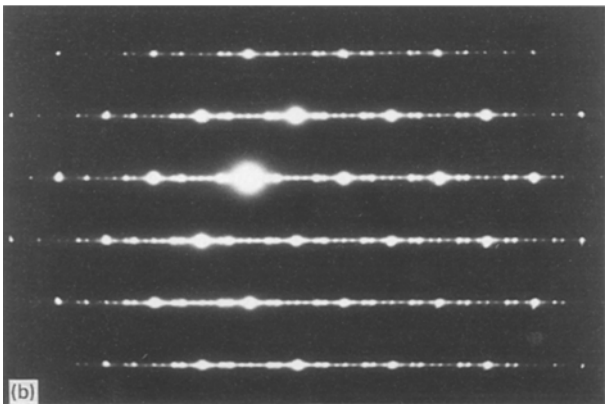

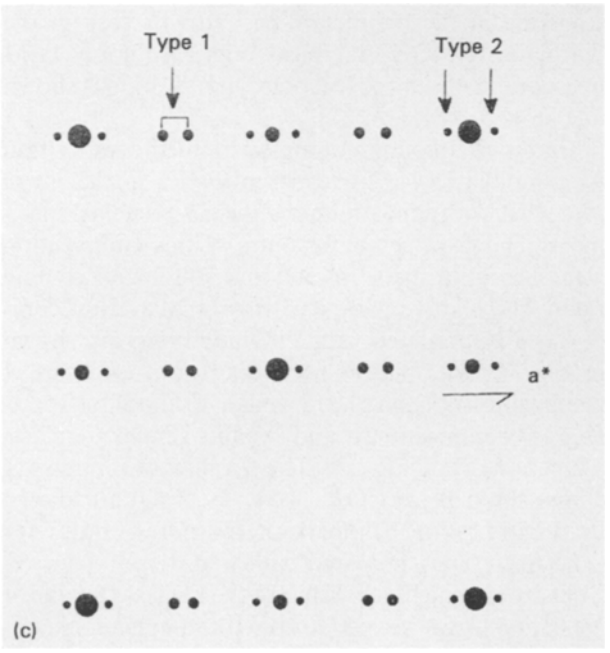

Figure 10 [0 1 1] electron diffraction patterns of ceramic of composition B: (a) air-quenched; (b) cooled at 1 °C h^{-1} after sintering; (c) schematic representation of the [0 1 1] electron diffraction pattern shown in Fig. 10(b).

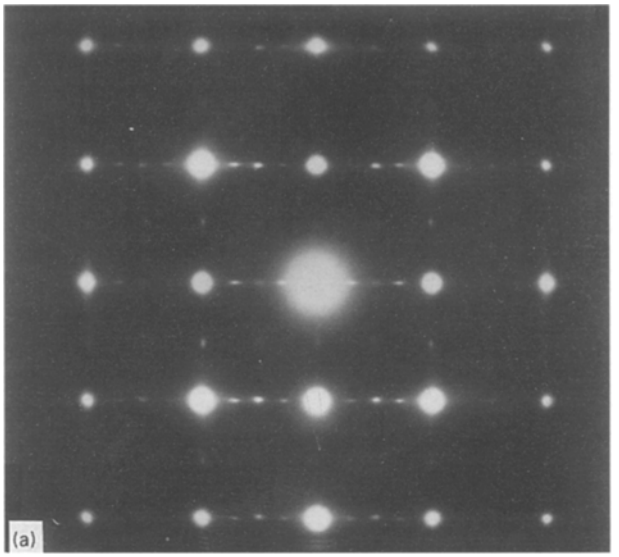

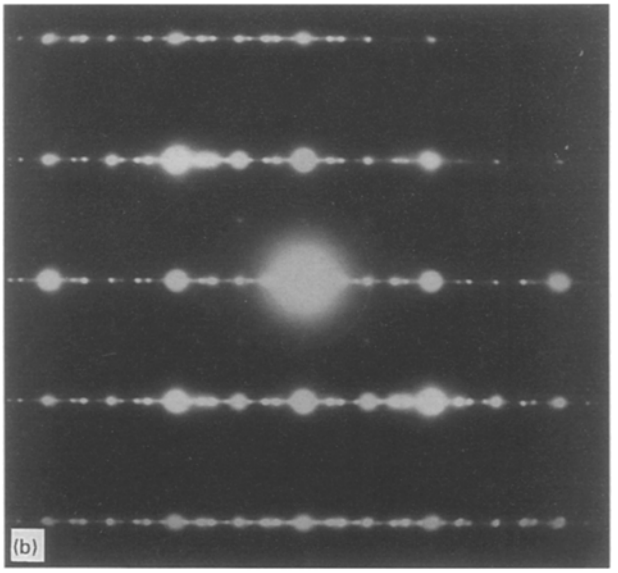

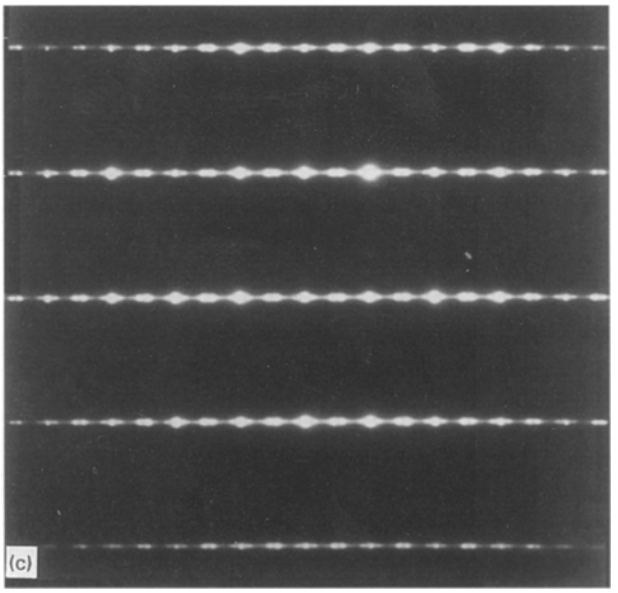

Figure 11 [0 1 2] electron diffraction patterns of ceramics of composition B: (a) cooled at 120 °C h^{-1}, (b) cooled at 6 °C h^{-1}, (c) cooled at 1 °C h^{-1} after sintering.

demonstrates the inability of ZT powders to sinter to acceptable high density by solid state diffusion. As a result of poor densification, the undoped ZT samples exhibited poor microwave dielectric properties; ε_r of 28 and dielectric Q values of less than 1000. The addition of 1.5 wt % ZnO or 2.5 wt % (ZnO + Y_2O_3 + CuO) promoted good densification (Fig. 1), and fired densities above 93% of the theoretical value were obtained for all specimens. The addition of ZnO improved densification through a liquid phase sintering mechanism, via the formation of a low melting temperature phase between ZnO and TiO_2. The

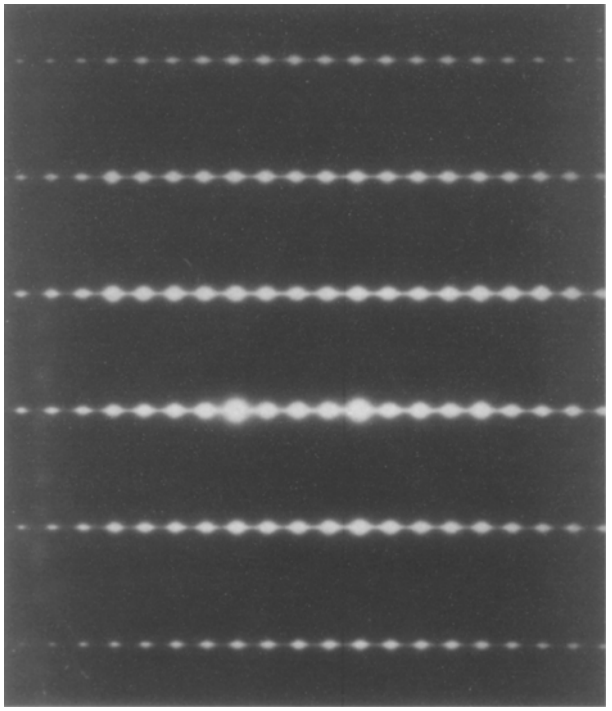

Figure 12 [0 1 2] electron diffraction pattern of ceramic of composition B, cooled at 1 °C h^{-1} after sintering and then annealed at 1000 °C for 1000 h. The diffraction pattern shows a superstructure with a doubled *a*-axis. Continuous streaking also exists in the *a*-direction.

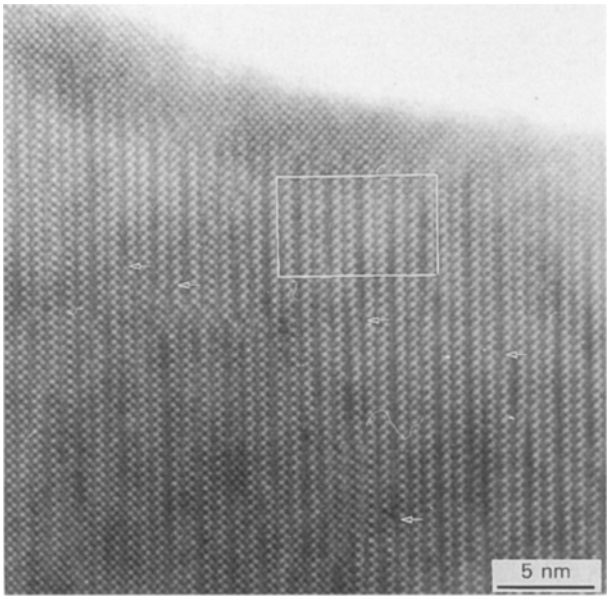

Figure 13 [0 0 1] TEM bright field image of sample of composition D cooled at 6 °C h^{-1}. The significance of the arrows, and the structural changes, are discussed in the text.

amount of the (Zn–Ti)-rich grain boundary phase decreased as the cooling rate was reduced. This can be understood in terms of the weight changes occurring at different cooling rates for the ZT samples. The undoped ZT ceramics showed a constant weight loss of 0.45 wt % at all cooling rates. ZrO_2 is not volatile at the sintering temperature of 1400 °C, and the weight loss may be due to volatile impurities which are present in the starting powder or organic species acquired during the milling process. The ZT ceramics prepared

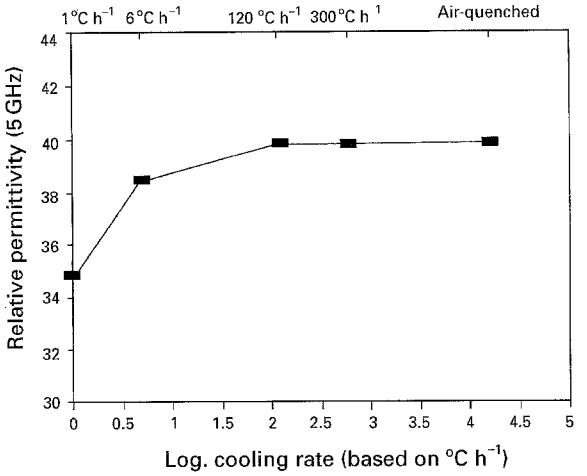

Figure 14 Relative permittivity (at 5 GHz) of ceramics of composition B (●) cooled at different rates after sintering. Individual ε_r values are believed to be reliable to ± 0.15.

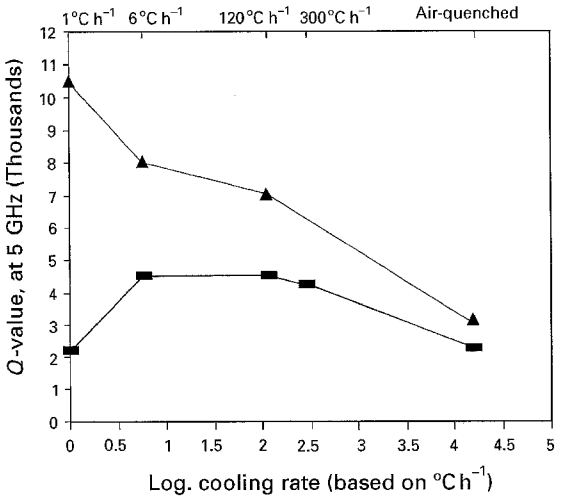

Figure 15 Dielectric *Q* values (at 5 GHz) for ceramics of composition B (■) cooled at different rates after sintering; data for $Zr_{0.8}Sn_{0.2}TiO_4$ (▲) (after Azough and Freer [7]) are included for comparison. Individual *Q* values are believed to be reliable to ± 300.

with ZnO additions showed higher weight loss values than the undoped ZT ceramics at all cooling rates. The difference in weight loss is most significant at cooling rates of 6 and 1 °C h^{-1} (0.75 and 1.9 wt % respectively). It is proposed that the weight loss is associated with the evaporation of ZnO during the sintering process. At the slowest cooling rates the samples are held at elevated temperatures for prolonged periods and the loss of ZnO is greatest. This proposal is consistent with the microstructural observations (Fig. 6(a)) which show that samples cooled at 1 °C h^{-1} contain only a residual trace of a (Zn–Ti)-rich grain boundary phase. In addition, the specimens cooled most slowly developed microcracks (Fig. 4(b)) and this almost certainly contributed to the reduction in density (Fig. 1).

The fired densities of ZT ceramics prepared with ZnO, Y_2O_3 and CuO additions are less dependent on cooling rate for the range air-quench to 6 °C h^{-1} (Fig. 1). This in part reflects the lower level of ZnO

in samples of composition D. Sintering samples at the higher temperature of 1450 °C enabled densities ~96% of theoretical to be obtained consistently. The presence of CuO, together with ZnO, appears to have improved densification via a liquid phase mechanism.

At a given cooling rate, ceramics of composition C exhibit the same density as specimens of composition B (Fig. 1), which indicates that Y_2O_3 additions do not play a significant role in the densification of ZT ceramics.

4.2. Order–disorder transformation in ZT ceramics

The contraction in the length of the *b*-axis as a function of cooling rate after sintering (Fig. 3) is believed to reflect an order–disorder transformation [11, 12] and electron diffraction studies have confirmed cation ordering in the *a*-direction. The [0 1 1] electron diffraction pattern of a rapidly cooled sample (Fig. 10(a)) shows only reflections from the fundamental-type lattice confirming that the high temperature form of zirconium titanate has a disordered structure. The [0 1 1] and [0 2 1] electron diffraction patterns of all samples cooled at 1 °C h^{-1} show two types of extra reflections in the *a*-direction (e.g. Figs. 10(b) and 11(c)). Fig.10 (c) is a schematic representation of the [0 1 1] diffraction pattern shown in Fig. 10(b). The extra spots can be associated with a superlattice in the *a* direction. The type 1 satellite reflections in Fig. 10(c) may be associated with the presence of an incommensurate superstructure in ordered zirconium titanate ($ZrTiO_4$). Christoffersen and Davis [16] suggested that such reflections arise from the presence of Zr–Zr–Ti–Ti–Zr–Zr (i.e. $ZZ^{TT}ZZ_{TT}$) and $Z^{TT}Z_{TT}$ sequences of cation layers within the structure. Type 2 reflections (Fig. 10(c)) are believed to reflect a degree of ordering of the distribution of the $ZZ^{TT}ZZ_{TT}$ and $Z^{TT}Z_{TT}$ structural regions [16, 17]. In the slowly cooled (1 °C h^{-1}) and annealed specimens, the electron diffraction pattern (Fig. 12) confirms the presence of an ordered superstructure with a doubled *a* axis. This electron diffraction pattern represents a commensurate-type superstructure for $ZrTiO_4$ and the figure exhibits many of the features obtained by Azough *et al.* [23] for $Zr_5Ti_7O_{24}$, which is the fully ordered form of zirconium titanate. However, even after annealing for 1000 h at 1000 °C, the present zirconium titanate specimen has not achieved a fully ordered form.

Fig. 13 is an [0 0 1] TEM bright field image of a sample of composition D cooled at 6 °C h^{-1}. Locations where individual layers of cations undergo a switch of occupancy are indicated by arrows. A number of cation stacking sequences were identified, including $ZZ^{TT}ZZ_{TT}$ and $Z^{TT}Z_{TT}$ as reported by Christoffersen and Davis [16, 17]. A region composed of the sequence $Z^{TT}ZZ_{TT}$ is outlined in Fig. 13. EDS analyses of the rapidly cooled (disordered) and slowly cooled (ordered) samples indicated no significant differences in sample chemistry: the Zr:Ti ratio being almost exactly 1:1.

Using an alternative approach Yamada *et al.* [14] examined the modulated structure of a low temperature form of $ZrTiO_4$ by X-ray diffraction and indexed the superstructure spots by introducing a modulated wave vector of $k = 0.58$. Electron density maps indicated the existence of a modulation of scattering amplitude of cations as well as a displacive modulation of oxygen ions.

4.3. Correlations between microstructure and microwave dielectric properties of ZT ceramics

The microstructures of the zirconium titanate ceramics shown in Figs 4–13 allow correlations between individual microstructural features and the microwave dielectric properties to be determined. Amongst the four compositions, the ZT + 1.5 wt % ZnO ceramics showed the highest dielectric *Q* values (Fig. 15) which are comparable with published data (Table III). The dielectric properties, and particularly the *Q* values, are thought to be affected by a combination of the following:

1. Grain boundary phases.
2. Microstructural defects (e.g. voids and microcracks).
3. Exsolution of a minor phase (e.g. Zr-rich particles).
4. Specimen density.
5. Grain size.
6. Order–disorder transformation.
7. Impurities and lattice defects.

The grain boundary phase in samples of composition B which were prepared with ZnO additions, is a (Zn–Ti)-rich phase. This is a low *Q* material and its presence as a grain boundary phase is detrimental to the dielectric properties at microwave frequencies [13]. For samples prepared with slow cooling rates, 6 and 1 °C h^{-1}, the high loss of ZnO led to a decrease in the amount of the (Zn–Ti)-rich phase and this should encourage a slight improvement in the *Q* value.

TABLE III Microwave dielectric properties of $ZrTiO_4$ ceramics

Frequency (GHz)	ε_r	*Q* value	$Q \times f$ (*f* in GHz)	Ref.
7	42	4000	28000	35
2.2	42	9000	19800	5
6	39	3700	22200	30
10	46	2700	27000	39
8.3	42.4	3079	25556	18 (Dis)
8.7	38.3	2280	19836	18 (Ord)
5	40.5	2000	10000	[a](Dis)
5	39.8	4500	22500	[b](Dis)
5	38.5	4500	22500	[c](Part)
5	34.9	2200	11000	[d](Ord)

[a] This study (composition B, air quenched)
[b] This study (composition B, cooled at 120 °C h^{-1})
[c] This study (composition B, cooled at 6 °C h^{-1})
[d] This study (composition B, cooled at 1 °C h^{-1}).
Ord = ordered specimen; Dis = disordered specimen; Part = partly ordered.

Slow cooling of the specimens leads to a structural distortion of the unit cell and individual grains. The shortening of the lattice parameter in the *b* direction, and the cell volume, eventually leads to the formation of microcracks (Fig. 7(b)), which occasionally coalesce to create voids at the grain boundaries (Fig. 9). These defects can have a deleterious effect on the dielectric Q value. The degrading effect of microcracks on the dielectric Q value of ceramics was acknowledged by O'Bryan *et al.* [24] for $BaTi_4O_9$ and $Ba_2Ti_9O_{20}$ ceramics. In these barium titanate ceramics the presence of microcracks caused a reduction in the dielectric Q values of at least 40%. The amount of microcracks in the ZT samples increased as a function of lattice contraction, in response to the reduction in the cooling rate. For samples cooled at $1\,^{\circ}C\,h^{-1}$ (Fig. 7(b)) the microstructure contains a high degree of microcracks, and thus in principle the so-called "low temperature" form of ZT would suffer a reduction of the dielectric Q value.

The exsolution of zirconia-rich particles (Figs 7(b), 8) can reduce the Q value in two different ways: the zirconia-rich phase is a low Q material [25] and the exsolution introduces microcracks within the grains (due to a volume expansion of ZrO_2 at the structural transition, $\sim 1000\,^{\circ}C$ [26]).

The increase in the grain size as the cooling rate was reduced is a general feature of all four compositions (Table I and Fig. 4(a–c)). It has been proposed that the grain size does not have a significant effect on the dielectric Q value. Iddles *et al.* [8] prepared a series of $Zr_{0.875}Ti_{0.875}Sn_{0.25}O_4$ ceramics doped with either La_2O_3 or Nb_2O_5 and found that the grain size increased with sintering time. This change was independent of Q value, especially for La-doped ceramics. They concluded that the grain size does not influence the Q value. Similarly, Ferreira *et al.* [27] found that the Q value was independent of grain size in magnesium titanate ceramics. As far as the authors are aware, there is no published report proposing the dependence of Q on grain size in any type of microwave ceramics. The present results for ZT ceramics support this proposal.

It may be expected that the residual porosity, which can be monitored by the fired density, will affect both ε_r and Q. In general terms the effect of porosity on relative permittivity can be estimated via the law of mixtures approach e.g. the Lichtenecker equation [28]

$$\log \varepsilon'_r = \sum_i \log \varepsilon_i V_i \qquad (1)$$

where ε'_r is the relative permittivity of the product, ε_i is the relative permittivity of the i^{th} phase, V_i is the volume fraction of the i^{th} phase and porosity is regarded as a phase with a relative permittivity of 1.

Increasing the amount of porosity will reduce the overall permittivity. Pores may also cause a reduction in Q, but the effect cannot be easily quantified. In the present study, porosity is not a significant problem as fired densities for compositions, B, C and D are above 93% of the theoretical value and, in general, specimen densities are independent of cooling rate (Fig. 1). The highest relative permittivity of 40.5 was obtained for air-quenched ZT samples prepared with ZnO additions (Fig. 14). The permittivities then decreased as the cooling rate decreased (Fig. 14 and Table III). This is consistent with the published data of Christoffersen *et al.* [18] for ordered and disordered ZT (Table III). With progressive ordering of the samples, there is a reduction in the molar volume and thus a reduction in the total polarizability which leads to a lowering of the relative permittivity [18]. For chemically prepared ZTS ceramics, Hirano *et al.* [29] found that ε_r increased with sintered density but the Q value was independent of density in the range 90–98% of theoretical density. However, for the ZT ceramics of this study the presence of microcracks, exsolved ZrO_2-rich particles with low relative permittivity [25] and reduction of cell volume are thought to be the main factors causing the reduction in the relative permittivities.

The final microstructural features which may influence the dielectric Q value are the degree of cation ordering and lattice defects. The water-quenched samples, which have the "high temperature" form of zirconium titanate, have a disordered structure, but because of the thermal shock the samples received during water quenching they fragmented and it is not possible to evaluate the Q values of such specimens. The air-quenched samples show the first stages of ordering. The presence of weak streaking in the *a*-direction (Fig. 10(a)), is associated with the initial stages of ordering and the samples may be regarded as the closest approximation to the high temperature form of zirconium titanate. These rapidly cooled specimens show low Q values of typically 2000 at 5 GHz. The disordered form of $ZrTiO_4$ possesses a low Q value. There was a significant increase in the dielectric Q values of ZT ceramics prepared with ZnO additions when the cooling rate was reduced to $300\,^{\circ}C\,h^{-1}$ (Fig. 15) and the Q value reached a maximum value for specimens cooled at a rate of $120\,^{\circ}C\,h^{-1}$. These samples show some degree of ordering (Fig. 11(a)). The degree of ordering increased further in specimens cooled at a rate of $6\,^{\circ}C\,h^{-1}$ (Fig. 11(b)) but there was no improvement in the dielectric Q value. The latter samples contain exsolved, low dielectric Q value, ZrO_2-rich particles and extensive microcracks. The fact that the specimens cooled at $6\,^{\circ}C\,h^{-1}$ have lower density (due to the higher porosity) but Q values almost comparable with that for specimens cooled at $120\,^{\circ}C\,h^{-1}$ suggests that the Q values are improved by ordering. The slowest cooled ($1\,^{\circ}C\,h^{-1}$) specimens show a high degree of order (Fig. 11c), but low Q values. The presence of extensive microcracks and the presence of a high quantity of exsolved ZrO_2-rich particle are responsible for the poor dielectric properties. The Q values of the slowly cooled ZT samples of composition B (prepared with ZnO additions) are higher than those for the air-quenched samples, which have an almost fully disordered structure.

The situation is generally much simpler for zirconium tin titanate (ZTS) ceramics. The presence of Sn in the zirconium titanate structure stabilizes the high temperature form [13, 29] and there is less change in the cell parameters as a function of the annealing

temperature or the cooling rate after sintering [7, 29]. By sintering ZTS ceramics in oxygen it is usually possible to achieve consistently high densities of $\geqslant 97\%$ of theoretical [7, 30]. Even with very slow cooling rates microcracking and exsolution are not major problems although the grain shape does become very distorted [7]. Azough and Freer [7] found a simple relationship between the dielectric Q values of $Zr_{0.8}Sn_{0.2}TiO_4$ ceramics and cooling rate after sintering (Fig. 15). The highest Q value of 10200 was obtained for specimens cooled slowly at $1\,^{\circ}C\,h^{-1}$ (exhibiting some degree of cation ordering). As specimens were cooled more rapidly the Q value decreased to the minimum of 3000 for air-quenched specimens (almost fully disordered).

In many complex perovskites, e.g. $Ba(Zn_{1/3}Ta_{2/3})O_3$ [31] and $Ba(Mg_{1/3}Ta_{2/3})O_3$ [32], cation ordering and elimination of the grain boundary phase has been shown to lead to a significant improvement of dielectric properties. The decrease in dielectric loss (i.e. increase in Q value by up to a factor of 10 for the complex perovskite ceramics), concurrent with increase in cation ordering, is believed to be caused by the reduction in lattice strain associated with the segregation of cations [31]. On the basis of these data, Christoffersen and Davies [17] argued that cation ordering in the zirconium titanate system should lead to significant reductions in dielectric loss. Subsequently, Christoffersen *et al.* [18] demonstrated that ordering of ZT ceramics causes an *increase* in dielectric loss, with Q values falling by approximately 30% (Table III). In contrast, Christoffersen *et al.* [18] noted that for the Sn doped ZT ceramics, e.g. $(Zr_{0.91}Sn_{0.09})TiO_4$, ordering had comparatively little effect on the dielectric Q values. Support for this latter observation comes from the recent study of Higuchi *et al.* [33] on ceramics of $(Zr_{0.8}Sn_{0.2})TiO_4$. They concluded that ordering has only a second order effect on the dielectric Q value of ZTS ceramics.

For a number of microwave dielectrics, Negas *et al.* [1, 34] noted that Q values are maximized if the grain boundaries are clean and overall impurity levels are minimized. Table III demonstrates that, with the exception of the preliminary data of Wakino *et al.* [35], the chemically prepared (and presumably the "cleanest") ZT samples of Hirano *et al.* [29] have the highest Q values (i.e. $Q \times f$ product of 27000). The control exercised by impurities/additives on the dielectric Q value appears to lie in the effect they have on the defect structure, particularly the type and concentration of defects generated. For example, with $Zr_{0.875}Ti_{0.875}Sn_{0.25}O_4$ ceramics Iddles *et al.* [8] found that the dielectric Q value of La-doped ZTS specimens showed a dramatic fall from 10000 to 3000 as the sintering time increased from 10 to 40 h. They explained this behaviour in terms of the diffusion of La ions into interstitial sites (La_i) in the host lattice (during prolonged sintering) generating electrons as the charge compensating species. In terms of standard Kroger–Vink notation [36], the reaction was described by

$$La_2O_3 \rightarrow 2La_i \cdots + 3/2\,O_2 + 6e'$$

Iddles and co-workers postulated that the additional electrons caused a decrease in the resistivity of the ceramic, mainfesting itself as a decrease in the dielectric Q value at microwave frequencies.

Wakino *et al.* [6] prepared ZTS ceramics containing small amounts of Fe_2O_3 and found that the presence of Fe_2O_3 in $Zr_{0.8}Sn_{0.2}TiO_4$ caused a degradation of the Q value. It was suggested that the Fe ions diffused into the lattice, possibly replacing Zr and/or Ti. The presence of the impurity ions in the host lattice modified the lattice vibration modes (which ultimately define ε_r and $\tan\delta$), and effectively reduced the Q value. Similar behaviour was noted by Azough and Freer [37] for ZTS ceramics containing small amounts of Cr_2O_3. As the Cr content increased the Q value fell. Azough and Freer [38] found that ZT ceramics prepared with Nd_2O_3 as a sintering aid (on the basis of a eutectic in the system TiO_2–Nd_2O_3 at 1380 °C [39]) had equally poor Q values (~ 700).

The same low Q values (600 to 800) were found for ZT + (1.5 wt % ZnO + 1.0 wt % Y_2O_3) and ZT + (1.0 wt % ZnO + 1.0 wt % Y_2O_3 + 0.5 wt % CuO) ceramics cooled at a variety of rates after sintering (compositions C and D). Since ZT + 1.5 wt % ZnO ceramics (composition B) possess high Q values and Y_2O_3 does not form a grain boundary phase in specimens of compositions C and D, it seems that Y_2O_3 also enters the ZT lattice and has a similar effect to the other trivalent ions in degrading the Q value. Clearly any benefit of potentially improving the ordering by the use of Y_2O_3 additions are outweighed by their detrimental effect on dielectric properties.

Wakino and Tamura [40] noted that large specimens of ZTS (e.g. 54 mm diameter and 24 mm thick) needed for 1 GHz resonators tend to suffer from lattice imperfections such as oxygen vacancies (manifested by a colour change from core to surface) causing lower Q values. Such defects are believed to be less important in small specimens.

More recently, Michiura *et al.* [41] examined the role of donor and acceptor ions in the dielectric loss of $Zr_{0.8}Sn_{0.2}TiO_4$ ceramics. The presence of 0.5 wt % Fe_2O_3 (with the Fe behaving as acceptors) caused the Q value of 7 GHz to fall from over 8000 to 810. The resulting concentration of Fe in the host ZTS grains was estimated to be ~ 4.3 mol %. To maintain charge neutrality in the ZTS lattice, there would be large numbers of Fe^{3+} ions and oxygen vacancies with effective charges of -1 and $+2$ respectively. Indeed, the lowering of the electrical resistivity to $10^{10}\,\Omega\,cm$ was considered to be due to imperfect compensation of Fe^{3+} ions and oxygen vacancies. In specimens prepared with 0.5 wt % Ta_2O_5 (the Ta behaving as donors), the dielectric Q value (8600) was marginally higher than that for the undoped reference material (8300). Sintering the Ta-doped samples in a reducing atmosphere had a minimal effect on the Q value, but the resistivity fell by five orders of magnitude. It was estimated that such samples contained 770 p.p.m. oxygen vacancies. In contrast, for the air-fired samples with the higher Q values, it was inferred that they contained lower concentrations of Ti^{3+} and oxygen vacancies. To interpret the variations in Q value and

electrical resistivity it was necessary to postulate the existence of tetravalent Ta with a localized electron. Therefore, free electrons and oxygen deficiency appear to be important factors which affect the Q values of ZT and ZTS ceramics.

The results obtained in this study and the observations of Iddles *et al.* [8], Wakino *et al.* [6] and Michiura *et al.* [41] strongly suggests that in zirconium–titanium–tin oxide ceramics the presence of elements with valency 3 (i.e. valency less than 4 which is the valency of the host Zr, Ti and Sn ions) in the lattice degrades the dielectric Q value. The presence of these trivalent elements appear to dominate the effect of other structural features such as ordering, grain size and grain boundary phases.

5. Conclusions

The microstructures and microwave dielectric properties of zirconium titanate ceramics are sensitive to the presence of additives and processing conditions. Specimens cooled rapidly after sintering are associated with a disordered microstructure. Reductions in the cooling rate lead to a reduction in the length of the lattice parameter in the b direction and the development of cation ordering. Although the dielectric Q values generally increased with the degree of cation ordering, the effect of ordering was overshadowed, and the Q value lowered by other microstructural features including the presence of (Zn–Ti)-rich grain boundary phases, exsolved zirconia nodules, microcracks and voids. In specimens cooled very slowly ($1\,^{\circ}C\,h^{-1}$) the (Zn–Ti)-rich grain boundary phase was eliminated by the evaporation of ZnO but there were significant microcracks and exsolved ZrO_2 which caused a lowering of the dielectric Q values. Specimen grain size increased as cooling rate decreased, but the Q values were independent of grain size.

The diffusion of trivalent impurities (yttria) into the host $ZrTiO_4$ grains also led to a lowering of the Q values. The presence of the impurities must have caused a modification of the lattice vibration modes, possibly via the development of lattice defects (oxygen vacancies).

In principle, the highest dielectric Q value (lowest dielectric loss) in zirconium titanate ceramics should be achieved in homogeneous specimens, free of trivalent impurities, in which low Q-value second phases, microcracks and deficiencies in oxygen are eliminated.

References

1. T. NEGAS, G. YEAGER, S. BELL and N. COATS, *Amer. Ceram. Soc. Bull.* **72** (1993) 80.
2. R. D. RICHTMYER, *J. Appl. Phys.* **10** (1939) 391.
3. J. K. PLOURDE and C. L. REN, *IEEE Trans. Microwave Theory Tech.* **MTT-29** (1981) 754.
4. R. FREER, *Silicate Industriels* **59** (1993) 191.
5. G. WOLFRAM and H. E. GOBEL, *Mater. Res. Bull.* **16** (1981) 1455.
6. K. WAKINO, K. MINAI and H. TAMURA, *J. Amer. Ceram. Soc.* **67** (1984) 278.
7. F. AZOUGH and R. FREER, in Proceedings of the 7th IEEE Symposium on application of ferroelectrics, June 1990, University of Illinois at Urbana-Champaign, USA, p. 198 (1991).
8. D. M. IDDLES, A. J. BELL and A. J. MOULSON, *J. Mater. Sci.* **27** (1992) 6303.
9. W. RATH, *Keram. Radsch.* **49** (1941) 137.
10. R. E. NEWNHAM, *J. Amer. Ceram. Soc.* **50** (1967) 216.
11. A. E. McHALE and R. S. ROTH, *ibid.* **66** (1983) C. 18.
12. *Idem., ibid.* **69** (1986) 827.
13. F. AZOUGH, Ph.D. Thesis, University of Manchester (1991).
14. T. YAMADA, K. URABE, H. IKAWA and H. SHIMOJIMA, *J. Ceram. Soc. Japan* **99** (1991) 380.
15. A. YAMAMOTO, K. TANAKA, H. MARUMO and HUKUNAGA, *Acta Crystallogr.* **47C** (1991) 1588.
16. R. CHRISTOFFERSEN and P. K. DAVIES, *J. Amer. Ceram. Soc.* **75** (1992) 563.
17. *Idem., Solid State Ionics* **57** (1992) 59.
18. R. CHRISTOFFERSEN, P. K. DAVIES and X. WEI, *J. Amer. Ceram. Soc.* **77** (1994) 1441.
19. S. C. CAMPBELL, US Patent 4,785,375 (1988).
20. M. I. MENDELSON, *J. Amer. Ceram. Soc.* **52** (1969) 443.
21. B. W. HAKKI and P. D. COLEMAN, *IRE Trans. on microwave theory and techniques MTT-8* (1960) 402.
22. D. HENNINGS and SCHNABEL, *Philips J. Res.* **38** (1983) 295.
23. F. AZOUGH, A. WRIGHT and R. FREER, *J. Solid State Chem.* **108** (1994) 294.
24. H. M. O'BRYAN, J. THOMSON and J. K. PLOURDE, *Ber Dt. Keram. Ges.* **55** (1978) 348.
25. G. H. JONKER and W. KWESTROO, *J. Amer. Ceram. Soc.* **41** (1958) 390.
26. R. C. GARVIE, in "High temperature oxides", part II, edited by A. M. Alper (Academic Press, New York, 1970) p. 117.
27. V. M. FERREIRA, F. AZOUGH, J. L. BAPTISTA and R. FREER, *Ferroelectrics* **133** (1992) 127.
28. K. LICHTENECKER, *Physik. Zeits.* **27** (1926) 833.
29. S.-I. HIRANO, T. HAYASHI and A. HATTORI, *J. Amer. Ceram. Soc.* **74** (1991) 1320.
30. P. C. OSBOND, R. W. WHATMORE, F. W. AINGER, *Brit. Ceram. Proc.* **36** (1985) 167.
31. S. KAWASHIMA, M. NISHIDA, I. UEDA and H. OUCHI, *J. Amer. Ceram. Soc.* **66** (1983) 421.
32. K. MATSUMOTO, K. TAKADA and H. IOKIMURA, in Proceedings of the sixth IEEE International symposium on applications of ferroelectrics, June 1986, Lehigh University, Pennsylvania, USA (1986) p. 118.
33. Y. HIGUCHI, N. MICHIURA, T. TATEKAWA and H. TAMURA, in "Ceramic Transactions Vol. 53, Materials and Processes for Wireless Communications," edited by T. Negas and H. Ling (Amer. Ceram. Soc., Westerville, OH) (1995) p. 153.
34. T. NEGAS, G. YEAGER, S. BELL and R. AMREN, in Proceedings of the International Conference on Chemistry of Electronic Ceramic Materials, held at Jackson WY, Aug. 1990 (NIST special publication 804, 1991) p. 21.
35. K. WAKINO, M. KATSUBE, H. TAMURA, N. NISHIKAWA and Y. ISHIKAWA, *Joint Conv. Record of 4th Inst. Elec. Eng. Japan* **285** (1976) 6.
36. F. A. KROGER and H. J. VINK, in "Solid state physics", Vol. 3, edited by F. Seitz and D. Turnbull (Academic Press Inc., New York, 1956) p. 307.
37. F. AZOUGH and R. FREER, *Brit. Ceram. Proc.* **42** (1989) 225.
38. *Idem.*, in Proceedings 1st European Ceramic Society Meeting, EUROCERAMICS, edited by G. de With, R. A. Terpstra and R. Metselaar, Vol. 2 (1989) p. 294.
39. A. V. ZAGORODNYUK, L. V. SADKOVSKAYA, G. V. SHAMRAI, I. P. KOVALEVSKAYA, R. L. MAGUNOV and G. A. TEFERIN, *Zh. Neorg. Khim.* **31** (1986) 2389.
40. K. WAKINO and H. TAMURA, In "Ceramic transactions Vol. 8, Ceramic Dielectrics: Composition, Processing and Properties" (edited by H. C. Ling and M. F. Yan) (American Ceramic Society, Westerville OH, 1990) p. 305.
41. N. MICHIURA, T. TATEKAWA, Y. HIGHUCHI and H. TAMURA, *J. Amer. Ceram. Soc.* **78** (1995) 793.

Received 21 August
and accepted 4 October 1995